Response to the reviewers

We thank the reviewers for their critical assessment of our work. In the following we address their concerns point by point which has helped to improve our manuscript. The reply below gives a motivation of the changes, as well as the additions to the manuscript (*in italic*). The figure numbers in the reply refer to the figures in the improved manuscript. All new and updated figures have been placed in the final section of the document, starting on page 23.

It is worth emphasizing that in response to Reviewer Point P 2.35, all simulations were re-run on a finer spatial grid. This updated resolution aligns with established literature (Lanzilao and Meyers, 2024; Maas and Raasch, 2022).

Reviewer 1

Review of "Wind farm blockage in convective boundary layers" written by O. Ndindayino and J. Meyers. This manuscript investigates the impact of blockage and gravity waves on 1.5 GW offshore wind farm under convective boundary layers, using ERA5 and LES. This study is relevant for understanding and optimizing the performance of future larger-scale offshore wind farms, particularly in relation to atmospheric stability effects. The manuscript would benefit from careful proofreading and more detailed explanations of key terms and methodological choices. Specific comments that authors should address are given below.

Reviewer Point P 1.1 — Abstract:
The abstract mainly summarizes the methods and results but does not clearly convey the motivation or the main contribution of the study. It is recommended that the authors restructure the abstract to:

- Begin with a broader background on wind farm blockage and its importance.
- Narrow down to the specific focus on convective boundary layers,
- Conclude with a clear statement of the novelty and significance of the findings.

Reply: Thank you for this valuable suggestion. The abstract has been thoroughly restructured to better articulate the motivation, specific scope, and novelty of the study. Following the recommended outline, the updated abstract is presented bellow:

As offshore wind farms grow in scale, their interactions with mesoscale atmospheric processes intensify, leading to significant wind farm blockage and the excitation of gravity waves that can heavily impact overall power production. While these phenomena have been extensively documented in stable and neutral atmospheric boundary layers, the influence of hydrostatic blockage within convective boundary layers (CBLs) remains underexplored and poorly understood. This study addresses this knowledge gap by investigating hydrostatic blockage within a large, 1.5 GW offshore wind farm operating under CBL conditions representative of marine cold air outbreaks (MCAO). Using high-fidelity large-eddy simulations (LESs) of a rectangular wind farm in staggered configuration, we analyze eight distinct scenarios by varying the capping-inversion (CI) height ($H = \{480, 980\}$ m) and the land-sea surface temperature difference ($\Delta\theta = \{0, 3, 6, 9\}$ K), which produce a diverse range of convective structures, *including rolls, intermediate forms, and cells. The results demonstrate that intensified convective mixing and buoyancy-driven turbulence driven by higher $\Delta\theta$ significantly accelerate wake recovery, leading to a more uniform power distribution and improved wake efficiency. At the same time, boundary layer growth slightly reduces the magnitude of both unfavourable and favourable pressure gradients, a sensitivity that is particularly pronounced in shallow boundary layers. Additionally, this study reveals that despite the enhanced turbulent mixing characteristic of highly convective regimes, the role of hydrostatic blockage and gravity waves persists as a dominant driver of wind farm performance, with front-row turbines suffering up to a 10% power deficit relative to free-standing turbines in deep boundary layers. These findings demonstrate that hydrostatic blockage persists in extreme convective regimes and must be integrated into wind farm design and performance modelling.*

Reviewer Point P 1.2 — Description of Atmospheric State:
The description of the atmospheric conditions lacks important details and justification:

- Which specific time period from ERA5 was used?
- Why is the analysis limited to wintertime? Is there prior research indicating that convective boundary layer conditions are representative or relevant during winter in this region?
- Among the eight cases listed in Table 2, why are the CI height and surface temperature difference emphasized? Please clarify the rationale and cite supporting literature if applicable.
- In Table 2, the four cases under H480 show slightly different values of H [m]. What explains these variations? The same question applies to H980.
- The value of $\Delta\theta 3$ is given as 2 K in Table 2. Please confirm whether this is correct.

Reply:

Thank you for raising this important point. The manuscript has been updated to include the missing information that answers the above questions:

- Which specific time period from ERA5 was used?
  Sect. 2.3 page 5: *Our analysis of the European Centre for Medium-Range Weather Forecasts Reanalysis v5 (ERA5) spanned a three-year period (2021–2023), focusing on full 24-hour cycles during the winter season.*
- Why is the analysis limited to wintertime? Is there prior research indicating that convective boundary layer conditions are representative or relevant during winter in this region?
  Sect. 2.3 page 5: *In alignment with findings by Fletcher et al. (2016), winter exhibits the most pronounced negative land–sea surface temperature differences ($\theta_l < \theta_s$), because land surfaces lose heat more rapidly than the sea during this season. These conditions trigger more frequent Marine Cold Air Outbreaks (MCAOs), leading to the development of convective boundary layers (CBLs) over the sea.*
- Among the eight cases listed in Table 2, why are the CI height and surface temperature difference emphasized? Please clarify the rationale and cite supporting literature if applicable.
  Sect. 2.3 page 6: *Due to computational limits, the parameter study is restricted to H and $\Delta\theta$. These parameters were selected because H directly influences the strength of the wind farm*

blockage, while $\Delta\theta$ dictates the convective strength through its direct connection to the surface heat flux.

- In Table 2, the four cases under H480 show slightly different values of H [m]. What explains these variations? The same question applies to H980.
  We have added the information that answers this question in two Sections.
  Sect. 2.4 page 8: *We therefore conclude that a statistical steady state is obtained after approximately $\Delta t_l = 16$ h. This equilibrium flow develops vertical profiles that differ slightly from the initial conditions. For instance, the resulting boundary layer height over land H_l slightly exceeds H_{init} due to vertical flow entrainment at the CI (Csanady, 1974).*
  Sect. 3 page 11: *Figure 4b, shows that H increases quasi-linearly with time for $\Delta\theta > 0$ k, similar to Lu and Porté-Agel (2015). This growth is driven by convective structures that generate turbulence, thereby enhancing the entrainment of flow from the free atmosphere into the boundary layer (Souaiby and Porté-Agel, 2025). Cases with identical H_l exhibit higher growth rates in H for larger $\Delta\theta$ as stronger convective structures are present in the CBL. Given the same $\Delta\theta$, shallower CBLs grow more rapidly due to the smaller volume of air below the CI. This confined volume allows sea-surface thermal plumes to form and reach the CI faster, which enhances the rate of vertical entrainment and promotes rapid CBL expansion.*

- The value of $\Delta\theta 3$ is given as 2 K in Table 2. Please confirm whether this is correct.
  We fixed this typo. the correct value is 3 K.

Reviewer Point P 1.3 — Section 2.4:
It is unclear whether the descriptions in the second paragraph of Section 2.4 are:

- Based on previously published studies, or
- Derived from results within this manuscript.

If these statements are based on prior work, appropriate references should be provided. If they are results from this study, the authors should explicitly point to the corresponding figures or sections that support these statements.

Reply: We have updated this paragraph for more clarity and consistency.

Sect. 2.4 page 9: *However, the precursor simulation results in Sect. 3 show that, the time constraints prevent the simulations from ever reaching this new CNBL state. Consequently, the CBL exhibits a slow transient evolution, characterized by a gradual increase in the boundary layer height H and a decrease in the surface kinematic heat flux q_w. Despite this transient, the simulations reach a period of constant thermal stability $-H/L_{ob}$, after approximately 1.5 h of spin-up (see Fig. 4c). During this interval, the velocity profiles shift from the super-geostrophic jet characteristic of the CNBL to the well-mixed profiles typically found in a CBL (see Fig. 5a). At the same time, a quasi-linear vertical heat flux profiles emerge (see Fig. 5d).*

Minor

Reviewer Point P 1.4 — There are instances where previously defined abbreviations are not consistently used, and terms are written out instead. Conversely, some abbreviations are used without prior definition. Please ensure that all abbreviations (e.g., LES, CBL) are properly defined and used consistently throughout the manuscript.

Reply: This has been fixed.

Reviewer Point P 1.5 — Similarly, some mathematical parameters are not defined (e.g., "g" in Eq. 1 and Figure 1). Please provide clear definitions for all variables.

Reply: We added the definitions of Eq. 1.

Sect. 1 page2: *... $g = 9.81$ m s^{-2} the gravitational acceleration and ...*

We also updated the caption of Fig. 1 to include the definition of all parameters present in the figure.

Reviewer Point P 1.6 — Figure 1: The color of the curve lines and the mathematical annotations is too light, making them difficult to read. Please use darker colors to improve visibility.

Reply: The colour has been changed, see Fig. 1.

Reviewer Point P 1.7 — Line 70: "ms^{-2}" → "m s^{-2}".

Reply: This typo has been fixed.

Reviewer Point P 1.8 — Section 2.1 lacks a discussion of the performance of the SP-Wind solver based on previous studies. Please include relevant references or a brief evaluation

Reply: We have rewritten the paragraph. Now we only include relevant references regarding the performance of the solver.

Sect. 2.1 page 5: *This in-house research code has been developed through the years, see amongst others Calaf et al. (2010); Allaerts and Meyers (2018); Lanzilao and Meyers (2024). Additionally, for code benchmarking, comparison and validation we refer to Martínez-Tossas et al. (2018); Sood et al. (2022); Ivanell et al. (2026).*

Reviewer Point P 1.9 — Please ensure consistent verb tense usage in Sections 2.2 and 2.3.

Reply: This has been updated.

Reviewer Point P 1.10 — ERA5 should be written out in full at its first occurrence, along with an appropriate reference.

Reply: This has been updated.

Sect. 2.3 page 5: *Our analysis of the European Centre for Medium-Range Weather Forecasts Reanalysis v5 (ERA5) spanned a three-year period (2021–2023), focusing on full 24-hour cycles during the winter season.*

Reviewer Point P 1.11 — Figure 3: Please clarify whether any comparison between LES results and ERA5 data has been considered or included.

Reply: Figure 3 (noted as Fig. 6 in this document) compares ERA5 data with the precursor LES. To improve the manuscript's logical flow, this figure was moved to Sec. 3, where it now accompanies the discussion on the resulting z-profiles of the precursor simulations.

Sect. 3 page 14: *In order to appraise the realism of our performed precursor LES, Fig. 2 compares the LES precursor temperature profiles (1 h time average) to the ERA5 data that fall within the red squares of Fig. 2. These regions are defined by intervals around the chosen parameter values:* $H \pm 150$ *m*, $\Delta\theta_{CI} \pm 1$ *K*, $\Delta h_{CI} \pm 150$ *m*, $\Gamma \pm 2$ *K km*$^{-1}$, *and* $\Delta\theta \pm 1$ *K*. .

Reviewer Point P 1.12 — In Line 115, Table 2 is referenced before Table 1. Please revise the order or swap the tables for consistency.

Reply: This has been fixed.

Reviewer Point P 1.13 — In Figure 2, the red rectangle has the same color as the red diamonds, making it difficult to distinguish between them. Please use different colors.

Reply: This has been fixed. The diamonds and dashed lines are now black.

Reviewer Point P 1.14 — In Figure 4, consider combining panels (a) and (b) into a single 3D box visualization, if appropriate.

Reply: Figure 4, now called Fig. 3 in the updated manuscript, has been changed into a single 3D sketch.

Reviewer Point P 1.15 — Line 160: Should this refer to "eight simulation cases" instead of "four cases"?

Reply: We thank the reviewer for this remark. Indeed this should refer to eight simulation cases. We have updated this

Reviewer Point P 1.16 — Line 188: "Fig. 6(d)" may need to be corrected to "Fig. 6(e)".

Reply: We thank the reviewer for pointing this out. This has been fixed

Reviewer Point P 1.17 — In Figure 6, are there explanations provided for panel (e)? Additionally, please clarify the meaning of the black and green dotted lines.

Reply: This has been updated. See previous point for description of panel (e). Additionally the meaning of the black and green dotted lines has been added to the caption:

The green dashed line denotes the turbine hub height while the black dashed lines are representative of the rotor dimension.

Reviewer Point P 1.18 — Are Figures 7 and 8 necessary? The flow results, including the wind farm region (x: 20–40 km, y: 15–25 km), could potentially be incorporated into Figure 9.

Reply:

We moved Fig. 9 (precursor flow field) to Sect. 3 earlier in the text, since this figure is solely about the atmospheric flow and not the wind farm. We chose to keep the 2D plots of the flow profiles around the farm as it nicely shows the evolution of the convective structures and wind farm wakes with increasing H and $\Delta\theta$.

Reviewer Point P 1.19 — In Figure 11, the y-axis scales in panels (a) and (b) should be aligned.

Reply: We thank the reviewer for this insightful remark. This has been fixed.

Reviewer Point P 1.20 — Line 306: The statement "Since variations in η_w are significantly larger than those in η_{nl}," is unclear. What is meant by "variations"? In Figure 14, the error bars for η_{nl} appear larger than those for η_w.

Reply: We updated this sentence:

Sect. 4.3 page 25: *The farm efficiency η_f follows the trend of η_w (Fig. 14c), as η_w exhibits significantly greater sensitivity to $\Delta\theta$ than η_{nl} does.*

Reviewer Point P 1.21 — Lines 331–333: Please clarify the differences between Π_1 and Π_3, as well as between Π_2 and Π_4.

Reply: We explained this as follows:

Sect 4.3 page 26: *This systematic isolation facilitates the attribution of the underlying mechanisms, namely pressure gradients and turbulent mixing, to the changes in the efficiencies. The efficiencies Π_1 and Π_3 capture changes in a, whereas Π_2 and Π_4 reflect changes in U_{in}. Specifically, Π_1 and Π_2 evaluate the difference between isolated and front-row turbines, while Π_3 and Π_4 compares the front row against the farm average. Although a and U_{in} depend on both mechanisms, the changes in the efficiencies can be confidently linked to one of the mechanisms, as demonstrated below.*

Reviewer 2

The paper investigates how wind farm performance varies depending on the surface temperature difference and boundary layer height of a CBL. In total eight cases are simulated using a spectral LES code and an actuator disc representation with constant loading. The CBL is created by running a CNBL precursor that then runs over a hotter surface with lower roughness.

The simulations and cases investigated are relevant, however at times it is difficult to follow and it remains unclear what the main aim is. A clear research question is missing, instead it remains strongly qualitative and descriptive with limited analysis. The paper is a clear progression of existing work from the group, however it does not really try to link up with previous work and show how a wind farm acts differently under a CBL compared to a CNBL. Whilst the title states that blockage is one of the main targets, no definition of blockage is provided, instead there is a large discussion on "efficiencies". It could be beneficial to review some work on blockage in neutral flows as well, as, especially with the higher boundary layer height, it might well be that one could just use simple blockage models to get the correct blockage. This would show that there is not additional pressure gradient caused by the interaction between farm and CBL. Also gravity waves and their importance are mentioned but without proof or analysis. Numerical sensitivities need to be investigated more thoroughly and the limitations of the study need to be made more clear (idealised turbine, idealised wind farm layout, idealised profiles, idealised wind direction).

Detailed comments are given in the attached document.

Reviewer Point P 2.1 — Line 1: Make sure to mention here and in other places that you are working on an idealised rectangular wind farm with a single wind direction

Reply: This is now emphesized.

Reviewer Point P 2.2 — Line 9–11: Hard to understand as the discussed efficiency measures have not been explained. More general statements that can easily understood would be preferable.

Reply: we updated the abstract to be more general:

The results demonstrate that intensified convective mixing and buoyancy-driven turbulence driven by higher $\Delta\theta$ significantly accelerate wake recovery, leading to a more uniform power distribution and improved wake efficiency. Concurrently, boundary layer growth slightly reduces the magnitude of both unfavourable and favourable pressure gradients, a sensitivity that is particularly pronounced in shallow boundary layers.

Reviewer Point P 2.3 — Line 11: This unsurprising in a stratified flow, the question is more whether they play a significant role.

Reply: We added more detail in the abstract:

Additionally, this study reveals that despite the enhanced turbulent mixing characteristic of highly convective regimes, the structural role of hydrostatic blockage and gravity waves persists as a dominant *driver of wind farm performance, with front-row turbines suffering up to a 10% power deficit relative to free-standing counterparts even in deep boundary layers.*

Reviewer Point P 2.4 — Line 19–20: Please also include work in your introduction and here from other groups than your own.

Reply: We have added more references:

Sect. 1 page 1: *High-fidelity numerical simulations have advanced the study of large semi-infinite and finite wind farms in stratified atmospheric boundary layers (ABLs). This includes investigations into stable boundary layers (SBLs) (Allaerts and Meyers, 2018; Strickland et al., 2022), conventional neutral boundary layers (CNBLs) (Allaerts and Meyers, 2017; Maas, 2023a,b; Lanzilao and Meyers, 2024; Stipa et al., 2024; Delvaux and Meyers, 2025), as well as studies covering both regimes (Maas and Raasch, 2022; Souaiby and Porté-Agel, 2025).*

Reviewer Point P 2.5 — Line 20: Important to mention that they are based on idealised rectangular wind farm layouts without mean wind direction changes.

Reply: We specify this now:

Sect. 1 page 1: *With the exception of Maas and Raasch (2022), who replicated the geometry of the German Exclusive Economic Zone, these prior studies analysed idealized rectangular wind farm layouts. Additionally all prior works evaluated single mean free stream wind direction perpendicular to the rotor planes at hub height.*

Reviewer Point P 2.6 — Line 21–22: Hard to follow if one has not read those publications. What is a favourable and unfavourable.

Reply: We have added more explanation:

Sect. 1 page 2: *The above mentioned studies have observed that momentum extraction by operating wind farms displaces the CI layer. This upward displacement, which acts as an interfacial gravity wave, elevates air with a lower potential temperature. The resulting cold anomaly creates a taller column of cold, dense air that locally increases pressure. Additionally, the CI displacement perturbs the free stratified atmosphere above, generating internal gravity waves. These three-dimensional waves also induce pressure perturbations that are felt throughout the atmospheric boundary layer (Smith, 2009). Combined, these two types of gravity waves establish pressure gradients both around and within the wind farm. The pressure gradient upstream of the farm significantly decelerates the incoming flow (often on the order of 10 % or more) and is consequently termed unfavourable (Δp_u). Conversely, the pressure gradient across the wind farm accelerates the flow through it, acting as a favourable gradient (Δp_f).*

Reviewer Point P 2.7 — Line 25: Hard to follow, maybe write out.

Reply: We updated this:

Sect. 1 page 2: *Additionally, Lanzilao and Meyers (2024) found that a stronger adverse pressure gradient strongly correlates with a decrease in non-local farm efficiency. Conversely, they reported a strong positive correlation between the favourable pressure gradient and the wind farm efficiency.*

Reviewer Point P 2.8 — Line 26: Make sure to define what you mean by blockage and blockage effects in the context of this study.

Reply: We have added a more clear explanation:

Sect. 1 page 2: *Following the definitions of Lanzilao and Meyers (2024), the upstream deceleration linked to CI displacement in stratified flow is defined as hydrostatic blockage. When combined with hydrodynamic blockage, defined as the collective induction of all individual turbines, the two mechanisms constitute the wind farm blockage. However, because wind farm blockage is heavily dominated by hydrostatic effects in stratified ABLs, these two terms are often used interchangeably. It should be noted that, the hydrostatic blockage is inherently coupled with the simultaneous internal flow acceleration driven by the favourable pressure gradient Δp_f in the farm itself.*

Reviewer Point P 2.9 — Line 27: What do you mean by that? Upstream wind losses do not necessarily lead to power losses as studies for single rows have shown.

Reply: We added more clarification:

Sect. 1 page 2: *In contrast, under CNBL, the favourable pressure gradient can offset the unfavourable pressure gradient losses, potentially improving efficiency compared to fully neutral ABL cases (Lanzilao and Meyers, 2024).*

Reviewer Point P 2.10 — Line 31: What type of LES study was this? Also wind farm related? Please elaborate. Also why did you use they definition?

Reply: We added more clarification:

Sect. 1 page 2: *Salesky et al. (2017) investigated the internal flow structures of CBLs across a suite of LESs with varying surface heat fluxes and geostrophic wind speeds. Their analysis identified three distinct regimes of convective organization and established that their occurrence is related to the thermal stability parameter $-H/L_{ob}$. This formulation is widely adopted in stratified atmospheric boundary layer research (Maas and Raasch, 2022; Souaiby and Porté-Agel, 2025).*

Reviewer Point P 2.11 — Line 33: What's that defined as? Inversion layer height?

Reply: Yes this is the inversion layer height. We added this to the manuscript:

Sect. 1 page 2: *Here H is the boundary layer height (equivalent to the CI height) and ...*

Reviewer Point P 2.12 — Line 43: So these studies included CBLs and what does "pronounced influence" mean here? On what?

Reply: We added a more precise explanation:

Sect. 1 page 3: *However the findings by Allaerts and Meyers (2018), Lanzilao and Meyers (2024) and Delvaux and Meyers (2025) indicate a significant influence of gravity waves and blockage effects on wind farm performance in CNBL. Consequently, this study aims to investigate whether these influences persist under the CBL conditions.*

Reviewer Point P 2.13 — Line 49–50: Please motivate why you choose to do it this way, there are also other options.

Reply: We added an explanation:

Sect. 1 page 4: *We opt for fixed surface temperatures as this inherently allows for decreasing surface heat fluxes over time, which occurs during the lifetime of a MCAO as it advects deeper into the open sea.*

Reviewer Point P 2.14 — Figure 1: Generally a nice figure, however make sure to define parameters in the text or caption and maybe use thicker font for the maths symbols, cyan is difficult to read

Reply: We updated Fig. 1, see reply to Reviewer Point P 1.5.

Reviewer Point P 2.15 — Line 69: Why this figure? (Mentioned later but should be mentioned here instead).

Reply: We have removed the numerical value from this sentence. Now the numerical value is present in Sect. 2.3 with the reasoning behind.

Sect. 2.3 page 5: *The ERA5 data corresponds to the coordinates 51.6°N, 3.0°E, representing the grid point closest to the Belgian–Dutch offshore wind farm cluster.*

Reviewer Point P 2.16 — Line 72: Generally I would recommend to put all these figures in the "simulation setup" section.

Reply: We have moved this numerical value to the Sect. 2.4 Simulation setup.

Reviewer Point P 2.17 — Line 74: Don't think this needs special mention and could be discussed together with the domain figures.

Reply: We have reduced the details:

Sect. 2.1 page 4: *The final term, f_i^{tot}, represents all external forces acting on the flow. This includes the wind turbine drag force, alongside the Rayleigh damping and fringe region forces detailed in the following sections.*

Reviewer Point P 2.18 — Line 78–80: Are all these references needed here? Do they contain developments of the code or are they examples where it has been used?
+
Line 86: Not sure all references are needed here.

Reply: We have rewritten the paragraph. Now we only include relevant references regarding the performance of the solver.

Sect. 2.1 page 5: *This in-house research code has been developed through the years, see amongst others Calaf et al. (2010); Allaerts and Meyers (2018); Lanzilao and Meyers (2024). Additionally, for* *code benchmarking, comparison and validation we refer to Martínez-Tossas et al. (2018); Sood et al. (2022); Ivanell et al. (2026).*

Reviewer Point P 2.19 — Line 91–92: Did you also use the same constants?

Reply: Yes, we explicitly specify this now:

Sect. 2.2 page 5: *To mitigate gravity wave reflections from this boundary, a Rayleigh damping layer (RDL) is implemented in the upper free atmosphere, adopting the methodology and parameter values of Lanzilao and Meyers (2023).*

Reviewer Point P 2.20 — Line 94: So wake effects are removed and not recycled?

Reply: Indeed. we have rephrased the paragraph to be more direct and clear:

Sect. 2.2 page 5: *Due to the pseudo-spectral nature of the solver, periodic boundary conditions are present in the horizontal directions. To break the periodicity in the streamwise direction and prescribe inflow conditions that prevent the recycling of turbine wakes, the wave-free fringe region technique of Lanzilao and Meyers (2023) is utilized. A body force is introduced to generate the desired inlet flow, while damping of vertical momentum above the ABL suppresses spurious gravity waves associated with this forcing (see Table 3 for spatial parameters). This method is used in combination with a concurrent precursor simulation, which continuously supplies a fully developed turbulent inflow field. The resulting wind farm domain is thus effectively infinitely wide, provided that farm-induced disturbances remain confined within its lateral boundaries.*

Reviewer Point P 2.21 — Line 98: Repetition

Reply: We removed the repetition and combined it with the first sentence where periodic boundary conditions are mentioned. See previous point.

Reviewer Point P 2.22 — Line 103: Why, please motivate.

Reply: We have added a motivation.

Sect. 2.3 page 5: *In alignment with findings by Fletcher et al. (2016), winter exhibits the most pronounced negative land–sea surface temperature differences ($\theta_l < \theta_s$), because land surfaces lose heat more rapidly than the sea during this season. These conditions trigger more frequent MCAOs, leading to the development of CBLs over the sea.*

Reviewer Point P 2.23 — Line 105: Please discuss the effect of vertical resolution on your results. ERA is rather coarse. Also did you use every 1 hour time stamp? Or did you reject some hours with respect to the goodness of the fit? Is it important how many years of ERA you take? A figure describing the different parameters you are fitting would help. Also indicate the uncertainty of the approach.

Reply: We updated the paragraph with multiple points. Regarding the three year analysis window:

Sect. 2.3 page 5: *While a longer analysis period could be considered, expanding the window from one to three years produces negligible shifts in the representative set of atmospheric CBL conditions.*

Regarding the vertical resolution:

Sect. 2.3 page 6: *The coarse vertical resolution of ERA5 relative to LES prevents SERZ from accurately fitting the surface layer (Δh_{SL})...*
Sect. 2.3 page 6: *It is worth noting that the ERA5 reanalysis maintains a relatively high temporal and spatial resolution for a global multiyear dataset, allowing for a decent representation of the vertical temperature profile's structure (Jamaer et al., 2023).*

Lastly, we added all the fitting parameters to Fig. 1.

The model estimates four key atmospheric parameters indicated in Fig. 1: the CI height (H), strength ($\Delta\theta_{CI}$), and thickness (Δh_{CI}), alongside the free atmospheric lapse rate (Γ).

Reviewer Point P 2.24 — Line 109: Hard to understand if one does not know the definition of the rampanelli profile.

Reply: We added additional explanation.

Sect. 2.3 page 6: *Therefore, the sea surface temperature θ_s was extracted directly from the ERA5 data and subtracted from the mixed-layer temperature θ_m (obtained from the SERZ model output) to determine the surface temperature jump $\Delta\theta$, where $\theta_l = \theta_m$.*

Reviewer Point P 2.25 — Line 113–114; 117: why?.

Reply:
We added a motivation.

Sect. 2.3 page 6: *The data were grouped into probability density functions to evaluate the relevant states (see Fig. 2). The chosen parameter values include $H = \{480,\ 980\}$ m, $\Delta\theta_{CI} = 6$ K, $\Delta h_{CI} = 300$ m, $\Gamma = 5$ K km^{-1}, and $\Delta\theta = \{0,\ 3,\ 6,\ 9\}$ K, where $\Delta\theta = 0$ K serves as the reference CNBL case. Consistent with Lanzilao and Meyers (2024), the geostrophic wind speed was fixed at $G = 10$ m s^{-1}, a value frequently observed at that location. Additionally, this value ensures that all turbines operate below their rated power, within a region where the thrust curve typically exhibits a relatively constant thrust coefficient. This selection results in a total of eight simulation cases, which are listed in Table 1. Due to computational limits, the parameter study is restricted to H and $\Delta\theta$. These parameters were selected because H directly influences the strength of the wind farm blockage, while $\Delta\theta$ dictates the CBL strength through its direct connection to the surface heat flux.*

Reviewer Point P 2.26 — Line 124: Motivate your choices, also for surface roughness.

Reply: We added a motivation.

Sect. 2.4 page 6: *This simulation models the flow over a land surface with a surface roughness length of $z_{0,l} = 1 \times 10^{-2}$ m, which is typical for open, flat terrain. The velocity field is initialized using* *a logarithmic profile with a friction velocity of $u_* = 0.28$ m s^{-1}, which approximates the expected u_* for the selected G, f_c, and $z_{0,l}$. Above the CI, this profile connects to a laminar geostrophic wind of $G = 10$ m s^{-1}.*

Reviewer Point P 2.27 — Line 126: How is that defined

Reply: We have added a paragraph that outlines the criterion used to define a statistically steady state.

Sect. 2.4 page 8: *A 16 h simulation over land shows that turbulent parameters stabilize during the final 2 hours. At hub height, the normalized standard deviations for momentum fluxes and horizontal velocity drop below 1 %, with remaining trends matching the scale of the fluctuations. We therefore conclude that a statistical steady state is obtained after approximately $\Delta t_l = 16$ h.*

Reviewer Point P 2.28 — Line 134: CBL?

Reply: We rephrased the sentence so that it is clear what we mean by a new steady-state CNBL.

Sect. 2.4 page 8: *The sea surface temperature remains fixed, while the overlying air mass travels across the sea and gradually warms up until a new steady-state CNBL is established. However, the precursor simulation results in Sect. 3 show that, the time constraints prevent the simulations from ever reaching this new CNBL state.*

Reviewer Point P 2.29 — Line 137: How is this checked?

Reply: We now refer to the corresponding Fig.

Sect. 2.4 page 8: *Despite this transient, the simulations reach a period of constant thermal stability $-H/L_{ob}$, after approximately 1.5 h of spin-up (see Fig. 4c).*

Reviewer Point P 2.30 — Figure 2: Nice figure but you need more details in the text on how the fitting was performed. See comment.

Reply: See reviewer point P2.23.

Reviewer Point P 2.31 — Figure 3: Hard to see the different profiles. Also the bottom left ERA data actually seems to be stable.

Reply: We have reduced the size of the markers in the graph.
Indeed a slightly stable case is possible since the plotted ERA5 in the figure corresponds with the parameter space from Fig. 2.

Sect. 3 page 14: *In order to appraise the realism of our performed precursor LES, Fig. 6 compares the LES precursor temperature profiles (1 h time average) to the ERA5 data that fall within the red squares of Fig. 2. These regions are defined by intervals around the chosen parameter values: $H \pm 150$ m, $\Delta\theta_{CI} \pm 1$ K, $\Delta h_{CI} \pm 150$ m, $\Gamma \pm 2$ K km^{-1}, and $\Delta\theta \pm 1$ K. The LES profiles correspond reasonably well to the ERA5 profiles.*

Reviewer Point P 2.32 — Line 147–148: Add reference. Also did you include the effect of prebend or did you remove it?

Reply: We now explicitly include references. Also prebend is not considered as we model turbine forces using actuator disk model

Sect. 2.5 page 9: *The setup considers an idealized, rectangular 1.5 GW offshore wind farm consisting of* $N_t = 100$ *non-rotating actuator disks (Meyers and Meneveau, 2010) modelled after the IEA 15 MW turbines (Gaertner et al., 2020b), each characterized by a rotor diameter* $D = 240$ *m and a hub height* $z_h = 150$ *m.*

Reviewer Point P 2.33 — Line 150: Maybe good to mention that this is rather dense.

Reply: We now mention this:

Sect. 2.5 page 9: *The turbines are arranged in a dense, staggered layout across 10 rows* (N_t^x) *and 10 columns* (N_t^y) *with a uniform streamwise and spanwise spacing of* $S_x = S_y = 5D$.

Reviewer Point P 2.34 — Line 151: Are you sure these hold also for CBLs? Some of your later figures seem to show significant changes parallel to the wind farm indicating that there is some acceleration all across the wind farm free region. It would be important to check whether you need greater spanwise extend.

Reply:

Due to the limited computational resources, we have chosen this specific domain size. However this is limited. We emphasise this now in the manuscript:

Sect. 2.5 page 10: *This leads to the following ratios* $L_{up}/L_f^x = 1.67$, $L_x/L_f^x = 4.63$, *and* $L_y/L_f^y = 3.51$. *These ratios are identical to the ones used in the wind farm CNBL study of Delvaux and Meyers (2025) and exceed the ratios used in the wind farm CBL study of Maas and Raasch (2022), making sure that artificial domain blockage is minimized.*

The flow acceleration at the sides of the wind farm are predominantly due the hydrostatic blockage triggered by the wind farm. We emphasise this now in the manuscript:

Sect. 4.1 page 15: *In the streamwise velocity fields, we observe for* $\Delta\theta = 0$ *the typical flow acceleration at the wind farm sides due to the favourable pressure gradient induced by blockage (Lanzilao and Meyers, 2024; Delvaux and Meyers, 2025). This acceleration is not an artefact of domain confinement, as it also manifests in simulations of wind farms in CNBLs utilizing exceptionally wide domains* $(L_y/L_f^y > 10)$*(Lanzilao and Meyers, 2025).*

Reviewer Point P 2.35 — Table 1: This seems rather coarse. Please discuss in the text, indicating studies that have shown that this is sufficient for a CBL, otherwise perform a grid study.

Reply: All simulations were re-run on a finer spatial grid. This updated resolution aligns with established literature (Lanzilao and Meyers, 2024; Maas and Raasch, 2022).

Sect. 2.4 page 6 *This simulation uses a horizontal grid resolution of* $\Delta x = 31.25$ *m and* $\Delta y = 21.74$ *m, alongside the stretched vertical grid specified in Table 2 (Lanzilao and Meyers, 2024). This resolution is comparable to that of the wind farm LESs in CBL conditions conducted by Maas and Raasch (2022).*

Reviewer Point P 2.36 — Table 1: Typo.

Reply: We fixed this.

Reviewer Point P 2.37 — Line 152: What is the hub height wind speed? The iea 15 actually pitches before reaching rated. It is also somewhat misleading to indicate that the iea15 was used, be precise, you only used the dimensions of the 15.

Reply: The paragraph was rephrased to accurately reflect the implementation details.

Sect. 2.5 page 9: *The setup considers an idealized, rectangular 1.5 GW offshore wind farm consisting of* $N_t = 100$ *non-rotating actuator disks (Meyers and Meneveau, 2010) modelled after the IEA 15 MW turbines (Gaertner et al., 2020b), each characterized by a rotor diameter* $D = 240$ *m and a hub height* $z_h = 150$ *m.*

...

Sect. 2.5 page 10: *Since the turbines operate below their rated power under the given conditions (hub height velocity* $M_{hub} \approx 10$ *m* s^{-1}*), we adopt a constant disc-based thrust coefficient* $C'_T = 1.44$ *as an input parameter for the simulations, which corresponds to* $C_T = 0.778$ *in the constant thrust region as obtained from the IEA 15 MW reference report (Gaertner et al., 2020a,b).*

Reviewer Point P 2.38 — Line 154–155: It should be mentioned somewhere that the wind direction at hub height is enforced to be aligned with x and by how much did the turbines have to yaw?

Reply: We added a specific description.

Sect. 2.4 page 9: *Note that the wind direction controller designed by Allaerts and Meyers (2015) is employed during all phases such that the flow is parallel to the x-axis at turbine hub height.*

We now also specify the maximum turbine yaw angle.

Sect. 2.5 page 11: *The maximum yaw angle measured is approximately* $9.64°$*.*

Reviewer Point P 2.39 — Table 2: How was this computed, averaging time and location.

Reply: We explicitly have added the methodology in the table caption.

Table 1. *Overview of the concurrent precursor simulations that drive the wind farm simulations. The parameters are horizontally and temporally averaged over a 1 h window following the 1.5 h spin-up phase.*

Reviewer Point P 2.40 — Line 160: I don't understand.

Reply: We added a more clear description.

Sect. 2.4 page 11: *To evaluate farm efficiencies, additional stand-alone turbine simulations are performed for each case within its corresponding atmospheric environment. Mitigating the impact of spatial heterogeneity on a single free-standing turbine requires averaging the outputs of several stand-alone units. Consequently, four turbines are uniformly spaced within a domain that matches the size of the concurrent precursor* ($L_x \times L_y \times L_z = 10$ *km* $\times 40$ *km* $\times 25$ *km*)*, allowing a representative average to be calculated. The turbine spacing (10 km) is sufficient to ensure they operate independently (Lanzilao and Meyers, 2024; Delvaux and Meyers, 2025).*

Reviewer Point P 2.41 — Line 163: This addresses in part one of my previous questions, please define H_0

Reply: We have changed the variable H_0 to H_textl as this would be more clear. Additionally we have added some clarification:

Sect. 3 page 11: *Figure 4 illustrates the temporal evolution of key boundary layer properties during both the spin-up and main phases of the concurrent precursor simulation. Specifically, panel (a) shows the horizontally averaged turbulence intensity at hub height* (TI_{hub})*, panel (b) displays the boundary layer height over sea* (H) *normalized by the height over land* (H_l)*, and panel (c) presents the stability parameter* ($-H/L_{ob}$)*.*

Reviewer Point P 2.42 — Figure 5: What is the influence of the continuously growing BL height?

Reply: We have added a more explicit explanation in the manuscript.

Sect. 3 page 11: *The increase in* H *within CBLs influences farm-induced blockage, as weaker pressure gradients are induced owing to reduced vertical confinement. However, this effect remains limited because the maximum increase in* H *is only* 10%*. A more extensive discussion is provided in Sect. 4*

We now emphasise the effect in Sect. 4.1 page 19:

When increasing $\Delta\theta$*, we observe a slight decrease in both pressure gradient magnitudes* $|\Delta p_u|$ *and* $|\Delta p_f|$*. However, this sensitivity is only noticeable for shallow boundary layers. This behaviour likely stems from the relatively larger increase in* H *observed in shallow cases as* $\Delta\theta$ *increases (see Fig. 4b).*

And in Sect. 4.3 page 26:

This trend is likely independent of enhanced turbulent mixing, which would typically exert a positive influence on the efficiencies. Rather, the behaviour of Π_3 *is driven by pressure gradients: the increase in* H *associated with higher* $\Delta\theta$ *mitigates farm blockage and weakens the favourable pressure gradient, thereby lowering the efficiency.*

Reviewer Point P 2.43 — Line 200: At what height? Hub height I suppose.

Reply: We now explicitly define the location in the text:

Sect. 4.1 page 15: *Figures 7 and 8 show the instantaneous streamwise and vertical velocity fields, at hub height, for all the tested atmospheric conditions.*

Reviewer Point P 2.44 — Line 203–204: Seems very similar to me, just the structures are different.

Reply: Indeed, this was poorly phrased. We updated the statement:

Sect. 4.1 page 15: *As $\Delta\theta$ increases, a similar flow speed-up occurs but is superimposed with convective structures.*

Reviewer Point P 2.45 — Line 212: At what height level? Also does the size change at different height levels? What about spectra at different locations and for the CNBL and CBL? What about gravity waves? How did you identify them and what is their magnitude? Are they interfacial or vertical? This needs more detailed discussion.

Reply: We thank the reviewer for these insightful comments. The paragraph detailing the convective structure size has been expanded to include additional information on how these structures were measured.

Sect. 3 page 15: *The surface layer ($z \leq \Delta h_{sl}$) is dominated by an abundance of small-scale updrafts. These updrafts merge within the mixed layer (defined as $\Delta h_{sl} \leq z \leq H - 0.5\Delta h_{CI}$, see Fig. 1) to form coherent convective structures that are capped by the CI. Within this mixed layer, λ remains roughly uniform in the vertical direction. Using a two-dimensional spatial Fourier transform of the vertical velocity field in the horizontal plane at hub height , we identify characteristic scales of $\lambda \approx 1.1$–1.2 km ($\lambda/H \approx 2.5$) for the shallow CBL cases, and $\lambda \approx 3.2$–3.3 km ($\lambda/H \approx 3.3$) for the deep CBL cases.*

We also added additional information related to the gravity wave excitation

Sect. 4.1 page 15: *Across all considered cases, the displacement of the CI by the wind farm, triggers gravity waves, as illustrated in Fig. 10. As discussed in Sect. 3 regarding Fig 5e, the convective structures beneath the CI generate weak gravity waves (Wulfmeyer et al., 2016). Fig. 10 demonstrates that the gravity waves in the convective H980-$\Delta\theta$9 case maintain a similar amplitude and frequency to those in the neutral H980-$\Delta\theta$0 case, but now the dominant wind farm induced waves are superimposed with the weaker gravity waves generated by the convective structures. Consequently, varying $\Delta\theta$ has no drastic impact on the resulting wave amplitude or wavelength. A more in-depth analysis of these gravity wave dynamics is provided by Lanzilao and Meyers (2024). We note that, the CBL parameters do not change significantly enough over the 1-hour wind farm analysis period to alter the induced gravity waves, indicating that these waves lack time-dependency on this timescale. Investigating much longer time horizons is beyond the scope of this study.*

Reviewer Point P 2.46 — Figure 10: One could also extract the BL height and discuss how that oscillates. Also what is happening towards the exit? That seems odd.

Reply:

We added the figure containing the CI displacement, see Fig. 11, as well as a fitting description in the manuscript:

Sect. 4.1 page 21: *Figure 11c displays the streamwise variation of the CI displacement, denoted as η. This displacement is defined as the difference between the CI height evaluated, using the SERZ model (Jamaer et al., 2023), in the concurrent precursor and the main domain. Shallow boundary layer cases exhibit a larger CI displacement, which is consistent with the stronger flow deceleration upstream and more pronounced pressure gradients shown in Figs. 11a and b. Furthermore, an increase in $\Delta\theta$ leads to greater CI displacement above the farm. As discussed in Sect. 3, this behaviour likely stems from a reduction in the CI strength $\Delta\theta_{CI}$, (Fig. 4). This weaker inversion offers less resistance, thereby allowing for larger displacements Smith (2009). Additionally, small interfacial waves are excited above and around the wind farm along the CI. The amplitude and frequency of these waves remain roughly independent of $\Delta\theta$, matching the observations in Fig. 10.*

Towards the end of the figure, the flow approaches the fringe region $x = 44.5$ km. We specify this now in the updated manuscript:

The plots are truncated at the start of the fringe region ($x_s^h = 44.5$ km). The sudden changes at the end of the profiles stem from the fringe region forcing, whose indirect influence extends only ≈ 2–3 km upstream into the domain.

Reviewer Point P 2.47 — Line 224–225: It would be nice to find those gravity waves and quantify them and then compare with CNBL cases. There has been previous work on shallow inversion layers and how that changes blockage / upstream pressure, please discuss. I am also wondering whether this are standing waves or is there a dependency on time here and does it change once we increase the domain size?

Reply: Similar results are found as in the CNBL cases of Lanzilao and Meyers (2024), where they also performed a domain sensitivity study. We also added a new plot that compares the gravity waves above wind farms in the CNBL with the CBL (Fig. 10):

Sect. 4.1 page 15: *Across all considered cases, the displacement of the CI by the wind farm, triggers internal and interfacial standing gravity waves, as illustrated in Fig. 10. As discussed in Sect. 3 regarding Fig 5e, the convective structures beneath the CI generate weak gravity waves (Wulfmeyer et al., 2016). Fig. 10 demonstrates that the gravity waves in the convective H980-$\Delta\theta 9$ case maintain a similar amplitude and frequency to those in the neutral H980-$\Delta\theta 0$ case, with the dominant wind farm induced waves now superimposed with the weaker gravity waves generated by the convective structures. Consequently, varying $\Delta\theta$ has no drastic impact on the resulting wave amplitude or wavelength. A more in-depth analysis of these gravity wave dynamics is provided by Lanzilao and Meyers (2024). We note that, the CBL parameters do not change significantly enough over the 1-hour wind farm analysis period to alter the induced gravity waves, indicating that these waves lack time-dependency on this timescale. Investigating much longer time horizons is beyond the scope of this study.*

Reviewer Point P 2.48 — Line 235: How do you define power here? You are not running a real turbine. Please define as you are probably using a very simplified way of computing it, ie using local disc averaged wind speed or something. In connection with that one needs to discuss that cp' is derived from a single turbine calibration which might not hold in a wind farm.

Reply: We explain are methodology more thoroughly.

Sect. 2.5 page 10: *The thrust force vector ($\mathbf{F}$) and power (P) for a single turbine are calculated as:*

$$\mathbf{F} = F\mathbf{e} = \frac{1}{2}\rho C_T' A_d U_d^2 \mathbf{e}, \tag{1}$$

$$P = FU_d = \frac{1}{2}\rho C_T' A_d U_d^3, \tag{2}$$

where $\mathbf{e}$ is the unit vector representing the turbine orientation, C_T' is the disc-based thrust coefficient, A_d is the rotor disk area and U_d is the disk averaged velocity normal to the rotor plane. Additionally, the Shapiro correction factor (Shapiro et al., 2019) is applied in U_d to prevent the overprediction of turbine power at typical LES grid resolutions. A further description of this implementation is given in Delvaux and Meyers (2025).

Reviewer Point P 2.49 — Line 235: How is the induction factor computed? This is not straightforward from a wind farm CFD simulation and needs to be discussed.

Reply: We refer to Appendix A.

Reviewer Point P 2.50 — Line 238: How could the first row be influenced by wakes at all? Please reformulate. Also downstream turbines are influenced by blockage, one cannot separate the two, one just cannot "see" the blockage anymore.

Reply: We rephrased this sentence for more clarity:

Sect. 4.2 page 20: *Consequently, the first two rows are free from wake effects and are instead dominated by blockage effects. This leads to a considerably smaller power deficit relative to the stand-alone turbine, in contrast to the remaining downstream rows where cumulative wake effects cause additional power losses.*

Reviewer Point P 2.51 — Line 243–244: So blockage is reduced.

Reply: Indeed, we rephrased the paragraph for more clarity.

Sect. 4.2 page 21: *Similar trends are observed for the shallow boundary layer (H480); however, in this regime, the transition from neutral to convective conditions does increase the normalized power of the first two rows. This behaviour is further elucidated by Fig. 10b, where the neutral case exhibits a more pronounced flow slowdown upstream of the farm, demonstrating that blockage is reduced when transitioning from neutral to convective conditions.*

Reviewer Point P 2.52 — Line 256: Please motivate why you looking at induction here.

Reply: We added a motivation.

Sect. 4.2 page 21: *To further highlight the impact of blockage-induced pressure gradients on turbine performance, Fig. 12c illustrates the row-averaged local axial induction, ...*

Reviewer Point P 2.53 — Line 258: There are methods for estimating Uin by measuring in several points inside the induction zone of a turbine using an induction zone model. This is rather straightforward and could be tried here.

Reply: We have added justification in the manuscript as to why we don't use the analytical models:

Appendix A: page 28: *Standard induction models were not used to extract local inflow conditions, as they neglect pressure gradients and thermal stratification. Instead, the LES data is analysed directly.*

Reviewer Point P 2.54 — Line 258: Confusing formulation.

Reply: We rephrased the sentence.

Sect. 4.2 page 21: *Increasing $\Delta\theta$ results in a lower axial induction factor for non-waked rows, whereas it drives an increase in the local axial induction for waked rows.*

Reviewer Point P 2.55 — Line 261: Are we sure then that by simulating with constant CT' we actually getting the correct turbine response here?

Reply: We added our motivation to the manuscript.

Sect. 2.5 page 10: *Prescribing a fixed C_T' neglects the dynamic response of the turbine, as the rotor is assumed to adjust instantaneously to the surrounding flow to maintain the targeted thrust set point. In reality, an actual turbine controller (e.g. a torque controller) considering rotor inertia, would modulate the turbine's response and performance. However, this dynamic effect is limited for mesoscale systems analysed here, given that the large-scale atmospheric time constants (e.g. gravity wave oscillations and convective structure propagation) are an order of magnitude larger than the turbine response time.*

Reviewer Point P 2.56 — Line 269–270: This has also been shown by neutral RANS simulations and experimental investigations studying blockage.

Reply: Indeed, we added this information.

Sect. 4.2 page 22: *Two distinct regimes emerge: high axial induction associated with low TI (green dashed box) and low axial induction associated with high TI (pink dash-dot box). This trend aligns with the turbine LES study across varying TI of Revaz and Porté-Agel (2025).*

Reviewer Point P 2.57 — Line 277: It would be interesting to see how this compares with recent work by some authors how pressure gradients influence single turbine power production.

Reply: We added a brief comparison to previous literature.

Sect. 4.2 page 21: *Additionally, this trend also aligns qualitatively with recent findings for single turbines operating within pressure gradients (Zengler et al., 2025; Ndindayino et al., 2025). In those* *studies, pressure gradients were induced either by deforming the vertical boundaries in the streamwise direction (Zengler et al., 2025) or by varying the domain confinement to introduce artificial blockage (Ndindayino et al., 2025). While the quasi-linear relationship between axial induction and the pressure gradient is successfully reproduced here, the curves do not match quantitatively. This discrepancy likely stems from differences in the simulated atmospheric conditions, as the present simulations resolve the CI instead of a rigid-lid boundary and include wind veer, as well as the inclusion of waked turbines.*

Reviewer Point P 2.58 — Line 280: Why are we doing this? Please motivate why we need to look at efficiencies and what they represent. Should we compare them to some reference?

Reply: We added an explanation.

Sect. 4.3 page 23: *Following Allaerts and Meyers (2018), by analysing the wind farm efficiencies we can further quantify how efficiently momentum is extracted by the turbines and how the induced pressure gradients and increased turbulent mixing affects the wind farm performance.*

Reviewer Point P 2.59 — Line 283: Can this not be simplified in your case? Are you suing $Cp'Ud^3$?

Reply: Yes indeed. We use the following formulation.

Sect. 4.3 page 23:

$$C_{\mathsf{P},mn} = C'_{\mathsf{T}} \left(\frac{U_{\mathsf{d},mn}}{U_\infty} \right)^3$$

Reviewer Point P 2.60 — Line 286: Might be better to show the difference with respect to an isolated turbine.

Reply: We now scale the C_P with the value of the isolated turbine in Fig. 14.

Reviewer Point P 2.61 — Line 291: Elaborate on what these efficiencies are trying to quantify.

Reply: We added an explanation.

Sect. 4.3 page 24: *These efficiencies enable a partial decoupling of the upstream flow deceleration from both the favourable pressure gradient and internal wake effects.*

Reviewer Point P 2.62 — Line 300–301: I don't see how this is surprising. Each turbine induces upstream wind speed reductions upstream also in neutral conditions, it is related to each turbine extracting momentum from the flow. It cannot disappear as then the turbines would not be present anymore. One would need a very strong external pressure gradient to remove it.

Reply:

We added an explanation.

Sect. 1 page 2: *Allaerts and Meyers (2018) demonstrated in their LES results, that a wind farm operating in an SBL experiences four times as much upstream flow deceleration (i.e., blockage) compared to the same wind farm operating in a CNBL under identical CI and free atmospheric conditions. This finding suggests that the opposite atmospheric state, the CBL, might drastically reduce the blockage effect. Specifically, enhanced wake recovery in CBLs could diminish the wind farm presence, thereby mitigating this effect.*

Reviewer Point P 2.63 — Line 331–333: I was about to mention why this is done, maybe this should be mentioned earlier. I am not sure I agree that we can split contributions like that. Pressure gradients influence wind speed as well.

Reply: We have mentioned the motivation behind the efficiency decoupling earlier in the paragraph now.
Indeed Pressure gradients influence wind speed as well. we have clarified the justification of the decomposition and got rid of inconsistencies in reasoning in this section.

Sect. 4.3 page 26: *This systematic isolation facilitates the attribution of the underlying mechanisms, namely pressure gradients and turbulent mixing, to the changes in the efficiencies. The efficiencies* Π_1 *and* Π_3 *capture changes in* a, *whereas* Π_2 *and* Π_4 *reflect changes in* U_{in}. *Specifically,* Π_1 *and* Π_2 *evaluate the difference between isolated and front-row turbines, while* Π_3 *and* Π_4 *compares the front row against the farm average. Although* a *and* U_{in} *depend on both mechanisms, the changes in the efficiencies can be confidently linked to one of the mechanisms, as demonstrated below.*

Reviewer Point P 2.64 — Line 354: Actuator discs with dimensions of the iea15.

Reply: We have changed this.

Sect. 5 page 27: *Using LESs performed with the SP-Wind solver, we analysed the performance of a 1.5 GW offshore wind farm consisting of 100 actuator disks with dimensions of the IEA 15 MW turbines operating inside a CBL.*

Reviewer Point P 2.65 — Line 374–375: I wouldn't say that this has been shown here. Is it really gravity waves that are the reason. Not just blockage due to a shallow semi-impermable lid? Waves were not really identified in this paper.

Reply: We thank the reviewer for this observation. Indeed the main focus was on the pressure gradients triggered by the displacement of the CI, which is typically considered as a two-dimensional interfacial gravity wave. Internal Gravity wave dynamics inside the free atmosphere were not investigated as much since similar flow fields were observed in the free atmosphere of CNBLS. We have added Fig. 10 and 11c to the manuscript as well as a discussion (see Reviewer Point P 2.46 and 2.47) in order support our claim. Additionally we have rephrased the sentence a bit for more clarity:

Sect. 5 page 28: *These findings emphasize that hydrostatic blockage and gravity wave excitation remain relevant even under more extreme convective regimes and should be incorporated into wind farm design and performance modelling.*

Figures

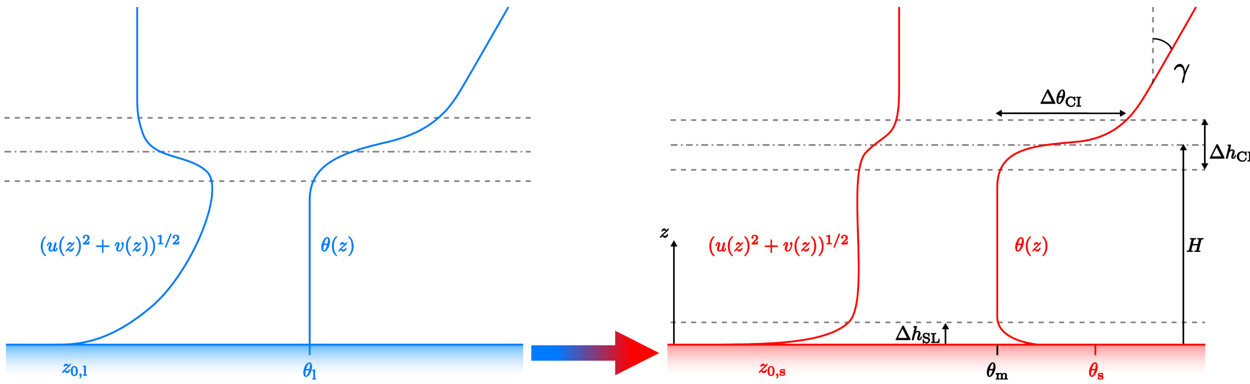

Figure 1. Schematic containing the vertical profiles of the horizontal velocity magnitude ($(u(z)^2 + v(z)^2)^{1/2}$) and potential temperature ($\theta(z)$) during a MCAO. The diagram illustrates the transition from land (with surface roughness $z_{0,\mathrm{l}}$ and temperature θ_l) to sea (with surface roughness $z_{0,\mathrm{s}}$ and temperature θ_s). The potential temperature profile also highlights the boundary layer height (H), the CI thickness (Δh_{CI}), the CI strength ($\Delta\theta_{\mathrm{CI}}$), the free-atmospheric lapse rate (Γ) and the surface layer thickness (Δh_{SL}). The left figure represents the flow over land simulated (with surface roughness $z_{0,\mathrm{l}}$ and temperature θ_l) in our computational domain, over a time interval $0 \to \Delta t_\mathrm{l}$. The right figure represents the flow over sea (with surface roughness $z_{0,\mathrm{s}}$ and temperature θ_s) simulated afterwards within the same domain over a time interval $\Delta t_\mathrm{l} \to \Delta t_\mathrm{l} + \Delta t_\mathrm{s}$.

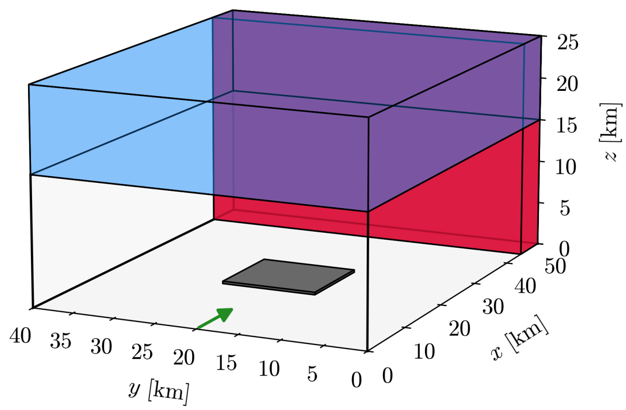

Figure 3. Schematic of the main domain. The blue and red boxes indicate the Rayleigh damping layer and fringe region, respectively. The wind farm is represented by the grey rectangle, with the green arrow denoting the flow direction at hub height.

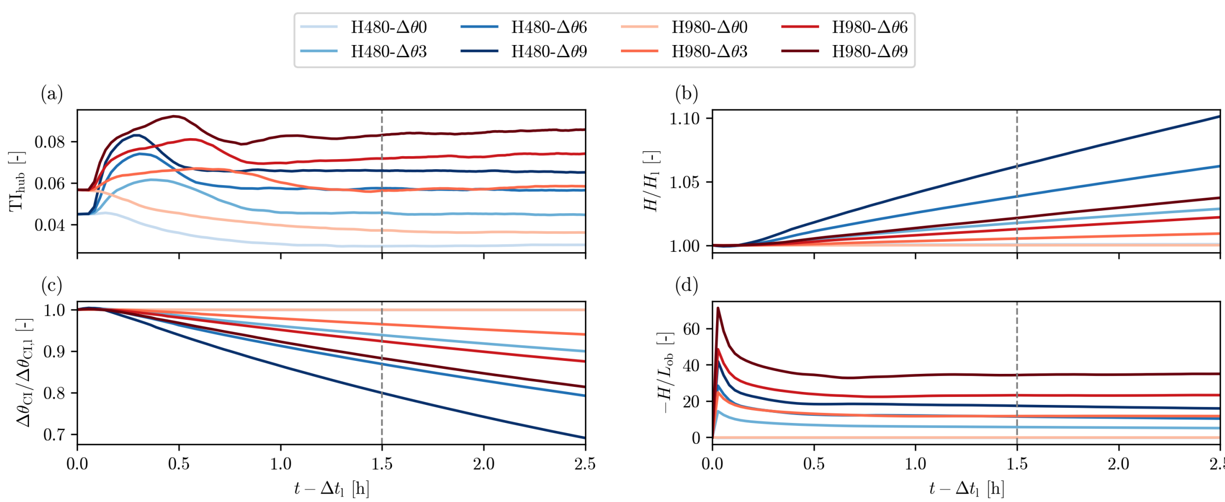

Figure 3. Temporal evolution above the sea surface of (a) the turbulence intensity at hub height, (b) the boundary layer height normalized the height over land, (c) the CI strength normalized by the strength over land and (d) the thermal stability parameter. The results cover the spin-up phase ($t - \Delta t_l \in [0, 1.5]$ h) and the main phase ($t - \Delta t_l \in [1.5, 2.5]$ h), separated by vertical grey dashed line.

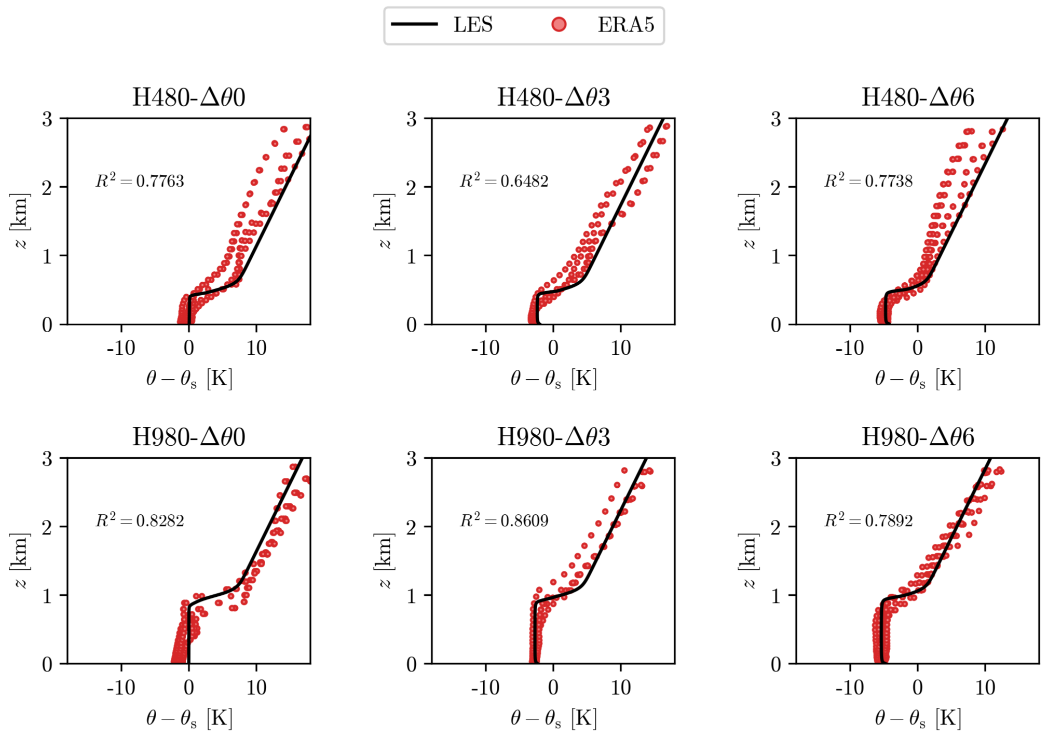

Figure 6. Comparison of vertical potential temperature profiles between precursor LES and ERA5 data. The solid black lines represent 1 h time-averaged LES results, while the red dots indicate five ERA5 profiles selected from the red rectangle parameter space defined in Fig. 2. The subplots display results for $H = \{480,\ 980\}$ m and $\Delta\theta = \{0,\ 3,\ 6\}$ K. The R^2 value denotes the coefficient of determination.

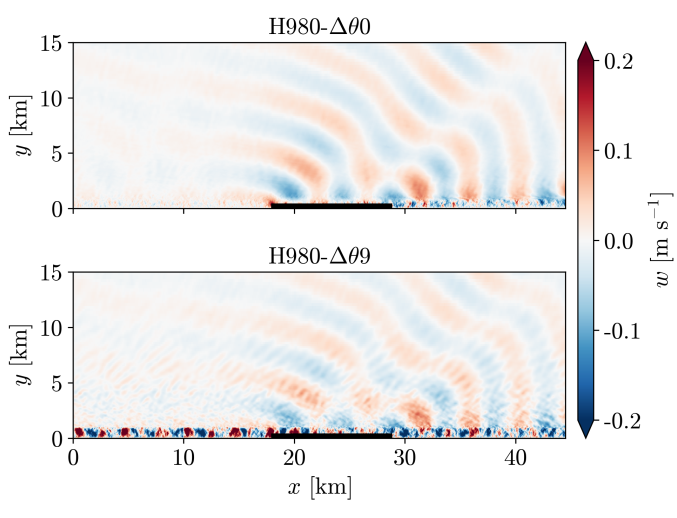

Figure 10. Instantaneous vertical (w) velocity fields in an x–z plane further averaged in the y direction along the width of the farm. The black box indicates the wind farm region.

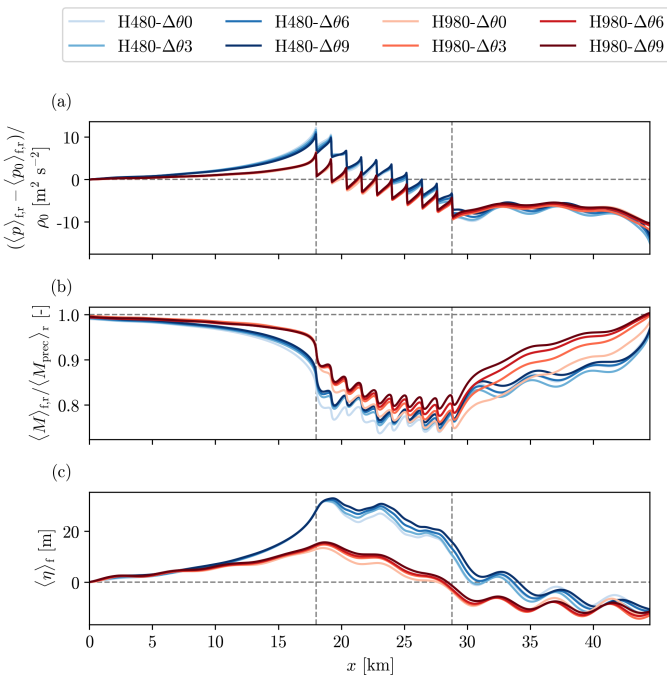

Figure 11. Time-averaged (a) pressure perturbation (b) horizontal velocity magnitude and (c) CI displacement averaged over the farm width as a function of the streamwise direction. The pressure and velocity are further averaged over the rotor height. The vertical dashed grey lines denote the location of the first- and last-row turbines.

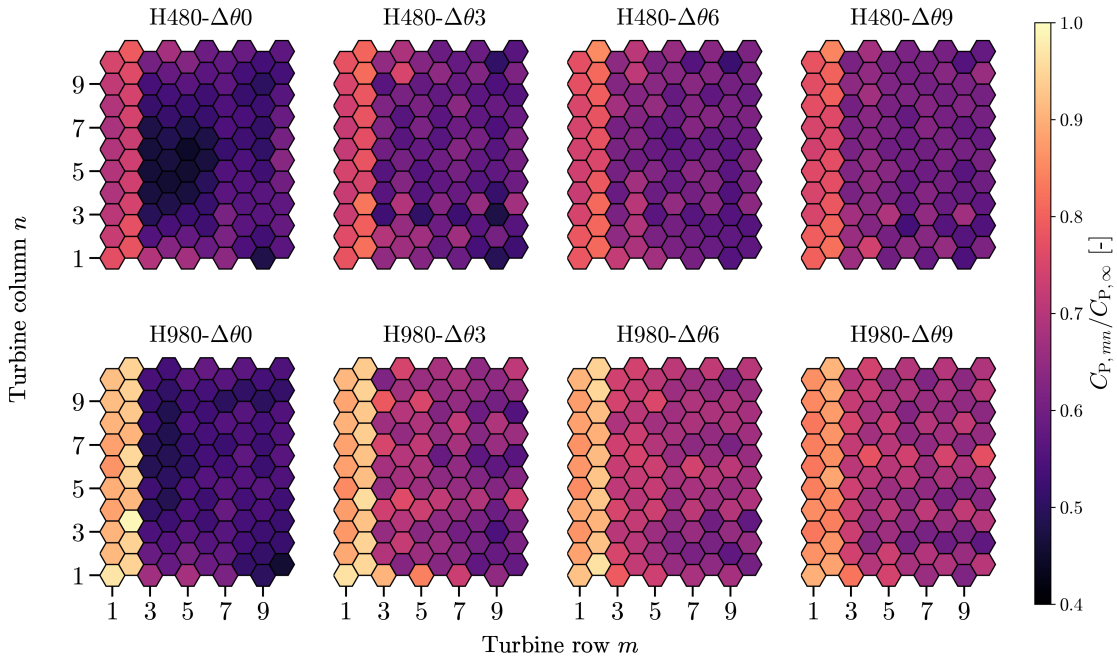

Figure 14. Spatial distribution of the turbine power coefficient ($C_{\mathrm{P},mn}$) across the wind farm from Eq. (9), normalized by the isolated turbine value ($C_{\mathrm{P},\infty}$).

References

Allaerts, D. and Meyers, J.: Large eddy simulation of a large wind-turbine array in a conventionally neutral atmospheric boundary layer, Physics of Fluids, 27, 065 108, https://doi.org/10.1063/1.4922339, 2015.

Allaerts, D. and Meyers, J.: Boundary-layer development and gravity waves in conventionally neutral wind farms, Journal of Fluid Mechanics, 814, 95–130, https://doi.org/10.1017/jfm.2017.11, 2017.

Allaerts, D. and Meyers, J.: Gravity Waves and Wind-Farm Efficiency in Neutral and Stable Conditions, Boundary-Layer Meteorology, 166, 269–299, https://doi.org/10.1007/s10546-017-0307-5, 2018.

Calaf, M., Meneveau, C., and Meyers, J.: Large eddy simulation study of fully developed wind-turbine array boundary layers, Physics of Fluids, 22, 015 110, https://doi.org/10.1063/1.3291077, 2010.

Csanady, G. T.: Equilibrium Theory of the Planetary Boundary Layer with an Inversion Lid, Boundary-Layer Meteorology, 6, 63–79, https://doi.org/10.1007/BF00232477, 1974.

Delvaux, T. and Meyers, J.: A large-eddy simulation analysis of collective wind farm axial-induction set points in the presence of blockage, Wind Energy Science, 10, 613–630, https://doi.org/10.5194/wes-10-613-2025, 2025.

Fletcher, J., Mason, S., and Jakob, C.: The Climatology, Meteorology, and Boundary Layer Structure of Marine Cold Air Outbreaks in Both Hemispheres, Journal of Climate, 29, 1999 – 2014, https://doi.org/10.1175/JCLI-D-15-0268.1, 2016.

Gaertner, E., Abbas, N., Barter, G., et al.: IEAWindSystems/IEA-15-240-RWT: Release v1.1.0, https://doi.org/10.5281/zenodo.3951793, 2020a.

Gaertner, E., Rinker, J., Sethuraman, L., et al.: Definition of the IEA 15-Megawatt Offshore Reference Wind Turbine, Tech. Rep. NREL/TP-5000-75698, National Renewable Energy Laboratory, Golden, CO, URL `https://www.nrel.gov/docs/fy20osti/75698.pdf`, 2020b.

Ivanell, S., Chanprasert, W., Lanzilao, L., Bleeg, J., Meyers, J., Mathieu, A., Juhl Andersen, S., Mouradi, R.-S., Dupont, E., Olivares-Espinosa, H., and Troldborg, N.: An inter-comparison study on the impact of atmospheric boundary layer height on gigawatt-scale wind plant performance, Wind Energy Science, 11, 937–960, https://doi.org/10.5194/wes-11-937-2026, 2026.

Jamaer, S., Allaerts, D., Meyers, J., and Lipzig, N. P. V.: A Novel Framework for Spatiotemporal Analysis of Temperature Profiles Applied to Europe, Journal of Applied Meteorology and Climatology, 62, 1855–1873, https://doi.org/10.1175/JAMC-D-22-0205.1, 2023.

Lanzilao, L. and Meyers, J.: An Improved Fringe-Region Technique for the Representation of Gravity Waves in Large Eddy Simulation with Application to Wind Farms, 2023.

Lanzilao, L. and Meyers, J.: A parametric large-eddy simulation study of wind-farm blockage and gravity waves in conventionally neutral boundary layers, Journal of Fluid Mechanics, 979, A54, https://doi.org/10.1017/jfm.2023.1088, 2024.

Lanzilao, L. and Meyers, J.: Wind-Farm Wake Recovery Mechanisms in Conventionally Neutral Boundary Layers, Journal of Fluid Mechanics, 1015, A5, https://doi.org/10.1017/jfm.2025.10320, 2025.

Lu, H. and Porté-Agel, F.: On the Impact of Wind Farms on a Convective Atmospheric Boundary Layer, Boundary-Layer Meteorology, 157, 81–96, https://doi.org/10.1007/s10546-015-0049-1, 2015.

Maas, O.: Large-eddy simulation of a 15 GW wind farm: Flow effects, energy budgets and comparison with wake models, Frontiers in Mechanical Engineering, Volume 9 - 2023, https://doi.org/10.3389/fmech.2023.1108180, 2023a.

Maas, O.: From gigawatt to multi-gigawatt wind farms: wake effects, energy budgets and inertial gravity waves investigated by large-eddy simulations, Wind Energy Science, 8, 535–556, https://doi.org/10.5194/wes-8-535-2023, 2023b.

Maas, O. and Raasch, S.: Wake properties and power output of very large wind farms for different meteorological conditions and turbine spacings: A large-eddy simulation case study for the German Bight, Wind Energy Science, 7, 715–739, https://doi.org/10.5194/wes-7-715-2022, 2022.

Martínez-Tossas, L. A., Churchfield, M. J., Yilmaz, A. E., Sarlak, H., Johnson, P. L., Sørensen, J. N., Meyers, J., and Meneveau, C.: Comparison of four large-eddy simulation research codes and effects of model coefficient and inflow turbulence in actuator-line-based wind turbine modeling, Journal of Renewable and Sustainable Energy, 10, 033 301, 2018.

Meyers, J. and Meneveau, C.: Large eddy simulations of large wind-turbine arrays in the atmospheric boundary layer, in: 48th AIAA Aerospace Sciences Meeting Including the New Horizons Forum and Aerospace Exposition, AIAA, Orlando, Florida, USA, https://doi.org/10.2514/6.2010-827, 2010.

Ndindayino, O., Puel, A., and Meyers, J.: Effect of Blockage on Wind Turbine Power and Wake Development, Wind Energy Science, 10, 2079–2098, https://doi.org/10.5194/wes-10-2079-2025, 2025.

Revaz, T. and Porté-Agel, F.: Effect of Turbulence Intensity on the Induction Factor and Power Efficiency of Wind Turbines, Wind Energy, 28, e70 040, https://doi.org/https://doi.org/10.1002/we.70040, e70040 we.70040, 2025.

Salesky, S., Chamecki, M., and Bou-Zeid, E.: On the Nature of the Transition Between Roll and Cellular Organization in the Convective Boundary Layer, Boundary-Layer Meteorology, 163, https://doi.org/10.1007/s10546-016-0220-3, 2017.

Shapiro, C. R., Gayme, D. F., and Meneveau, C.: Filtered actuator disks: Theory and application to wind turbine models in large eddy simulation, Wind Energy, 22, 1414–1420, https://doi.org/https://doi.org/10.1002/we.2376, 2019.

Smith, R.: Gravity wave effects on wind farm efficiency, Wind Energy, 13, 449 – 458, https://doi.org/10.1002/we.366, 2009.

Sood, I., Simon, E., Vitsas, A., Blockmans, B., Larsen, G. C., and Meyers, J.: Comparison of large eddy simulations against measurements from the Lillgrund offshore wind farm, Wind Energy Science, 7, 2469–2489, https://doi.org/10.5194/wes-7-2469-2022, 2022.

Souaiby, M. and Porté-Agel, F.: Atmospheric stability effect on wind farm flow and performance, Physics of Fluids, 37, 095 152, https://doi.org/10.1063/5.0280027, 2025.

Stipa, S., Ajay, A., Allaerts, D., and Brinkerhoff, J.: TOSCA – an open-source, finite-volume, large-eddy simulation (LES) environment for wind farm flows, Wind Energy Science, 9, 297–320, https://doi.org/10.5194/wes-9-297-2024, 2024.

Strickland, J. M., Gadde, S. N., and Stevens, R. J.: Wind farm blockage in a stable atmospheric boundary layer, Renewable Energy, 197, 50–58, https://doi.org/https://doi.org/10.1016/j.renene.2022.07.108, 2022.

Wulfmeyer, V., Muppa, S. K., Behrendt, A., Hammann, E., Späth, F., Sorbjan, Z., Turner, D. D., and Hardesty, R. M.: Determination of Convective Boundary Layer Entrainment Fluxes, Dissipation Rates, and the Molecular Destruction of Variances: Theoretical Description and a Strategy for Its Confirmation with a Novel Lidar System Synergy, Journal of the Atmospheric Sciences, 73, 667 – 692, https://doi.org/10.1175/JAS-D-14-0392.1, 2016.

Zengler, C. P., Troldborg, N., and Gaunaa, M.: Modeling the Influence of Streamwise Flow Field Acceleration on the Aerodynamic Performance of an Actuator Disk, Wind Energy Science, 10, 1485–1497, https://doi.org/10.5194/wes-10-1485-2025, 2025.